Boundary discrete time crystals induced by topological superconductors in solvable spin chains

Peng Xu [1] and Tian-Shu Deng [2,3,*]

[1] *School of Physics, Zhengzhou University, Zhengzhou 450001, China*
[2] *School of Physics and Astronomy, Yunnan University, Kunming 650091, China*
[3] *Institute for Advanced Study, Tsinghua University, Beijing 100084, China*

(Received 3 November 2022; revised 17 February 2023; accepted 17 February 2023; published 1 March 2023)

The Floquet time crystal, which breaks discrete time-translation symmetry, is an intriguing phenomenon in nonequilibrium systems. It is crucial to understand the rigidity and robustness of discrete time crystal (DTC) phases in a many-body system, and finding a precisely solvable model can pave a way for understanding of the DTC phase. Here, we propose and study a solvable spin chain model by mapping it to a Floquet superconductor through the Jordan-Wigner transformation. The phase diagrams of Floquet topological systems are characterized by topological invariants and tell the existence of anomalous edge states. The subharmonic oscillation, which is the typical signal of the DTC, can be generated from such edge states and protected by topology and solvability. We also examine the robustness of the DTC by adding symmetry-preserving and symmetry-breaking perturbations. Our results on the topologically protected DTC can provide a deep understanding of the DTC when generalized to other interacting or dissipative systems.

DOI: 10.1103/PhysRevB.107.104301

I. INTRODUCTION

Periodic driving is a powerful tool to engineer a variety of unique and fascinating phenomena in many-body systems, such as the Mott-insulator–superfluid transition [1], dynamical gauge field [2,3], many-body echo [4,5], and realization of topological band structures [6,7]. Recently, Floquet systems have also brought new possibilities to simulate time-translation symmetry broken phases, which are called discrete time crystals (DTCs), and this has attracted much attention from both experimentalists [8–18] and theorists [19–26]. The concept of the time crystal was originally proposed by Wilczek [27]. However, it was ruled out by the no-go theorem in thermal equilibrium systems [28,29]. Then, Khemani *et al.* [19] and Else *et al.* [20] generalized the concept of the time crystal and proposed the DTC, which exhibits a unique property that the expectation values of generic observables manifest a subharmonic oscillation. For example, the kicked Ising chain model with disordered interaction, where spins collectively flip after one period and back to their initial state after two periods, is a canonical realization of the DTC.

In a noninteracting spin chain system, taking $\hat{U} = \exp(-i\theta \sum_j \hat{X}_j)$ with $\theta = \pi/2$ as a Floquet evolution operator is a straightforward method to flip all spins in one period. Here, $\hat{X}_j$ is a spin operator acting on site j. However, when θ deviates slightly from $\pi/2$, the period of observables also deviates from twice the Floquet period. This means that the subharmonic response induced by $\hat{U} = \exp(-i\theta \sum_j \hat{X}_j)$ is a fine-tuned result and easily destroyed by perturbations. This simple example implies that the robustness of subharmonic response is a crucial property of the DTC. According to the previous results, many-body localization and prethermalization may provide two mechanisms to stabilize the subharmonic response in closed systems, while in open quantum systems, the dissipative discrete time crystal also exists, which could be explained by Floquet dynamical symmetry [25,30,31] and the mean-field approach [12,32]. Besides, topologically protected anomalous edge states [33–35] also suggest another mechanism of generating the robust DTC and the reasons are listed in the following. First, edge states in topological insulators (superconductors) are protected by symmetries. As long as the symmetries are not broken and the gap does not close, topological edge states are stable and robust. Second, Floquet topological insulators (superconductors) host anomalous edge states with quasienergy π/T which can generate a subharmonic response to driving frequency $2\pi/T$. Although the relation between π-mode edge states in Floquet topological system and the DTC has been discussed in previous research [19,36–44], detailed and systematic studies of topologically protected DTCs in a more general spin chain model are still lacking. Bridging Floquet topological superconductors to the topologically protected DTC in a general periodically driven spin chain model and explicitly analyzing the dynamics of observables are significantly helpful for deeply understanding the existence and robustness of the DTC. In our setup, the observable of a topologically protected time crystal is localized around the boundary, which can be called boundary discrete time crystals. It is worth mentioning that boundary time crystals have been discussed a great deal in previous studies [17,45–49]. Furthermore, we believe our topologically solvable model will also bring new inspiration in the research of boundary time crystals.

In this work, we investigate the existence of the DTC phase in a general Floquet spin chain model. Such a periodically driven spin chain can be mapped to a Floquet superconductor

*tianshudeng500@gmail.com

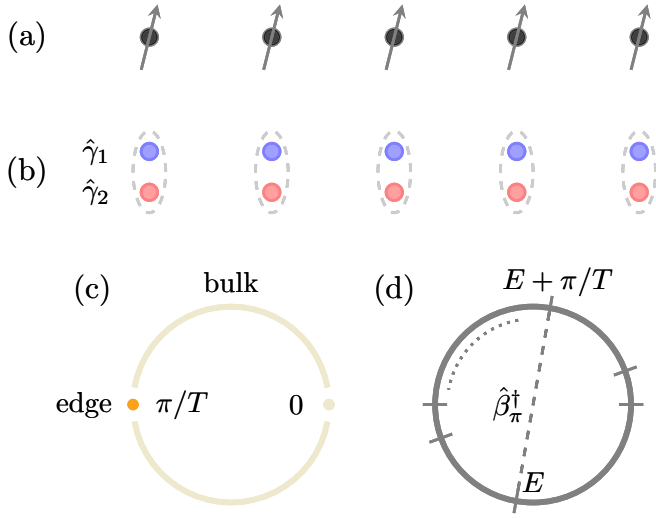

FIG. 1. (a) Schematic of spin chain. (b) Schematic of Majorana chain. (c) Quasienergy spectrum $\exp(-i\epsilon_\mu T)$ with ϵ_μ the quasienergy excitation. 0 and π/T represent two edge states' quasienergy excitations. (d) Eigenvalues of the Floquet evolution operator $\hat{U}_T$. Quasiparticle operator $\hat{\beta}^\dagger_\pi$ excites a state $|E\rangle$ with eigenenergy E to another state $|E+\pi/T\rangle$.

through the Jordan-Wigner transformation, after which the model becomes the form of a fermionic model. This model is intrinsic with particle-hole symmetry. Furthermore, this system can be classified into D class or BDI class [50], which is dependent on whether chiral symmetry is preserved. The topological Floquet superconductor exhibit a special kind of topologically nontrivial phase, where anomalous edge states with quasienergy π/T exist. In order to observe a robust DTC, the observable should be selected as the anomalous edge mode or the end spin. We numerically demonstrate that both observables manifest a subharmonic response with a generic initial product state. Finally, we also confirm the robustness of the DTC by adding symmetry-preserving and symmetry-breaking perturbations.

The paper is organized as follows. In Sec. II, we describe a general periodically driven spin chain model and map it to a Floquet superconductor. In Sec. III, we discuss the topological classification of this model, calculate the topological invariants, and obtain the phase diagrams. In Sec. IV, we demonstrate the existence of the DTC resulting from the Floquet superconductors, by selecting the observable as the anomalous edge mode or the end spin. Finally, in Sec. V, we examine how the robustness of the DTC is protected by the topologically nontrivial phase by adding symmetry-preserving and symmetry-breaking perturbations.

II. MODEL: PERIODICALLY DRIVEN SPIN CHAIN

We consider a periodically driven spin-1/2 chain as illustrated in Fig. 1(a),

$$\hat{H}(t)=\begin{cases}\hat{H}_1, & \text{for} \quad nT\leqslant t<nT+t_1,\\ \hat{H}_2, & \text{for} \quad nT+t_1\leqslant t<(n+1)T,\end{cases} \tag{1}$$

where

$$\hat{H}_m=J_m^{xx}\sum_j\hat{X}_j\hat{X}_{j+1}+J_m^{yy}\sum_j\hat{Y}_j\hat{Y}_{j+1}+J_m^{xy}\sum_j\hat{X}_j\hat{Y}_{j+1}+J_m^{yx}\sum_j\hat{Y}_j\hat{X}_{j+1}+h_m^z\sum_j\hat{Z}_j. \tag{2}$$

$\hat{X}_j$, $\hat{Y}_j$, and $\hat{Z}_j$ are spin operators (with the form of Pauli matrices) acting on the jth site. Here, $m=1,2$ represents the mth interval of the Hamiltonian $\hat{H}(t)$ in Eq. (2). And the chain contains N spins. J_m^{xx}, J_m^{yy}, J_m^{xy}, J_m^{yx} represent the strengths of nearest spin interactions and h_m^z the transverse field during the mth time interval. By employing the Jordan-Wigner transformation,

$$\begin{aligned}\hat{X}_j&=(\hat{c}_j^\dagger+\hat{c}_j)e^{i\pi\sum_{l<j}\hat{c}_l^\dagger\hat{c}_l},\\ \hat{Y}_j&=-i(\hat{c}_j^\dagger-\hat{c}_j)e^{i\pi\sum_{l<j}\hat{c}_l^\dagger\hat{c}_l},\\ \hat{Z}_j&=2\hat{c}_j^\dagger\hat{c}_j-1,\end{aligned} \tag{3}$$

where $\hat{c}_j^\dagger$ and $\hat{c}_j$ are the creation and annihilation fermion operators on the jth site. Then the Hamiltonian in Eq. (2) can be mapped to a fermionic system,

$$\begin{aligned}\hat{H}_m=&\sum_j\left(J_m^{xx}-J_m^{yy}-iJ_m^{xy}-iJ_m^{yx}\right)\hat{c}_j^\dagger\hat{c}_{j+1}^\dagger\\&+\sum_j\left(J_m^{xx}+J_m^{yy}+iJ_m^{xy}-iJ_m^{yx}\right)\hat{c}_j^\dagger\hat{c}_{j+1}\\&+\frac{h_m^z}{2}\sum_j(2\hat{c}_j^\dagger\hat{c}_j-1)+\text{H.c.}\end{aligned} \tag{4}$$

Furthermore, by defining $\hat{\gamma}_{j,1}=\frac{1}{\sqrt{2}}(\hat{c}_j^\dagger+\hat{c}_j)$ and $\hat{\gamma}_{j,2}=i\frac{1}{\sqrt{2}}(\hat{c}_j-\hat{c}_j^\dagger)$, we obtain a Hamiltonian in Majorana representation, as illustrated in Fig. 1(b),

$$\begin{aligned}\hat{H}_m=&2J_m^{xx}\sum_j i\hat{\gamma}_{j,2}\hat{\gamma}_{j+1,1}-2J_m^{yy}\sum_j i\hat{\gamma}_{j,1}\hat{\gamma}_{j+1,2}\\&+2J_m^{xy}\sum_j i\hat{\gamma}_{j,2}\hat{\gamma}_{j+1,2}-2J_m^{yx}\sum_j i\hat{\gamma}_{j,1}\hat{\gamma}_{j+1,1}\\&+2J_m^z\sum_j i\hat{\gamma}_{j,2}\hat{\gamma}_{j,1}.\end{aligned} \tag{5}$$

Both Hamiltonians $\hat{H}_1$ and $\hat{H}_2$ in Eq. (5) are quadratic, so they can be rewritten as

$$\hat{H}_m=\tfrac{1}{2}\hat{\Psi}^\dagger H_m\hat{\Psi}, \tag{6}$$

with

$$\hat{\Psi}^\dagger=(\hat{\gamma}_{1,1}\quad\hat{\gamma}_{1,2}\quad\hat{\gamma}_{2,1}\quad\hat{\gamma}_{2,2}\quad\ldots), \tag{7}$$

where H_m is a $2N\times 2N$ antisymmetric matrix. Here and after, $\hat{H}$ ($\hat{U}$) represents an operator and H (U) represents a matrix. Applying the Fourier transformation $\hat{\gamma}_{j,m}=\frac{1}{\sqrt{N}}\sum_k\hat{\gamma}_{k,m}e^{ikj}$, $\hat{H}_m(k)$ has such a form

$$\hat{H}_m=\sum_k(\hat{\gamma}_{k,1}^\dagger\quad\hat{\gamma}_{k,2}^\dagger)\left[d_m^0(k)I+\boldsymbol{d}_m(k)\cdot\boldsymbol{\sigma}\right]\begin{pmatrix}\hat{\gamma}_{k,1}\\ \hat{\gamma}_{k,2}\end{pmatrix}, \tag{8}$$

where $\boldsymbol{\sigma} = (\sigma_x, \sigma_y, \sigma_z)$ denote Pauli matrices. $d_m^0(k)$ and $\boldsymbol{d}_m(k)$ are given by

$$\begin{aligned} d_m^0(k) &= \left(J_m^{yx} - J_m^{xy}\right)\sin(k), \\ d_m^x(k) &= \left(J_m^{yy} - J_m^{xx}\right)\sin(k), \\ d_m^y(k) &= J_m^z + \left(J_m^{xx} + J_m^{yy}\right)\cos(k), \\ d_m^z(k) &= \left(J_m^{xy} + J_m^{yx}\right)\sin(k). \end{aligned} \tag{9}$$

For the periodically driven Hamiltonian in Eq. (1), the Floquet evolution operator $\hat{U}_T$ and the effective Hamiltonian $\hat{H}_{\text{eff}}$ are defined by

$$\begin{aligned} \hat{U}_T &= \hat{\mathcal{T}}\exp\left(-i\int_0^T \hat{H}(t)dt\right) = \exp(-i\hat{H}_2 t_2)\exp(-i\hat{H}_1 t_1) \\ &= \exp(-i\hat{H}_{\text{eff}}T), \end{aligned} \tag{10}$$

where $t_2 = T - t_1$. Based on the quadratic form of $\hat{H}_1$ and $\hat{H}_2$ in Eq. (5), we have proven in Appendix A that the Floquet effective Hamiltonian is also quadratic, which means $\hat{H}_{\text{eff}}$ also takes the form

$$\hat{H}_{\text{eff}} = \tfrac{1}{2}\hat{\Psi}^\dagger H_{\text{eff}}\hat{\Psi}. \tag{11}$$

In order to obtain the eigenenergies of $\hat{H}_{\text{eff}}$, we diagonalize the above matrix H_{eff} in real space as

$$H_{\text{eff}} = V\Lambda^\epsilon V^\dagger, \tag{12}$$

where

$$V = (|V_1\rangle \quad |V_2\rangle \quad \cdots \quad |V_{2N}\rangle), \tag{13}$$

$$\Lambda = \begin{pmatrix} \epsilon_1 & & & \\ & \epsilon_2 & & \\ & & \ddots & \\ & & & \epsilon_{2N} \end{pmatrix}. \tag{14}$$

$|V_\mu\rangle$ is the eigenvector of H_{eff} with eigenvalue ϵ_μ such that $H_{\text{eff}}|V_\mu\rangle = \epsilon_\mu|V_\mu\rangle$. ϵ_μ is the Bogoliubov quasiparticle excitation spectrum of $\hat{H}_{\text{eff}}$, which is restricted to the Floquet Brillouin zone $[-\pi/T, \pi/T)$. Then, the Floquet effective Hamiltonian $\hat{H}_{\text{eff}}$ in this quasiparticle representation can be rewritten as

$$\hat{H}_{\text{eff}} = \tfrac{1}{2}\hat{\Psi}^\dagger V\Lambda^\epsilon V^\dagger\hat{\Psi} = \tfrac{1}{2}\hat{\Phi}^\dagger\Lambda^\epsilon\hat{\Phi}, \tag{15}$$

where $\hat{\Phi}$ is composed of Bogoliubov quasiparticles $\hat{\Phi}^\dagger = (\hat{\alpha}_1^\dagger \quad \hat{\alpha}_2^\dagger \quad \cdots \quad \hat{\alpha}_{2N}^\dagger)$ and $\hat{\alpha}_\mu^\dagger = \hat{\Psi}^\dagger|V_\mu\rangle$.

Due to the particle-hole symmetry constraint, the eigenvalues and eigenvectors of H_{eff} must come in the pair

$$\begin{aligned} H_{\text{eff}}|V_\mu\rangle &= \epsilon_\mu|V_\mu\rangle, \\ H_{\text{eff}}|V_\mu^*\rangle &= -\epsilon_\mu|V_\mu^*\rangle. \end{aligned} \tag{16}$$

For $\epsilon_\mu = 0$ and π/T, this property also holds and the eigenstates will degenerate. The degree of degeneracy must be even when the dimension of the Hilbert space is even. Substituting these relations into Eq. (15), the effective Hamiltonian $\hat{H}_{\text{eff}}$ becomes

$$\hat{H}_{\text{eff}} = \sum_{\epsilon_\mu>0}\epsilon_\mu\left(\hat{\alpha}_\mu^\dagger\hat{\alpha}_\mu - \frac{1}{2}\right). \tag{17}$$

The eigenstate of $\hat{H}_{\text{eff}}$ is given by $\prod_\mu|n_\mu\rangle = (\alpha_\mu^\dagger)^{n_\mu}|0\rangle$. $n_\mu = 0, 1$ represents the number of occupations on the quasiparticle mode. Then the energy spectrum of this system can be expressed as

$$\begin{aligned} E &= \langle\hat{H}_{\text{eff}}\rangle \\ &= \sum_{\epsilon_\mu>0}\epsilon_\mu\left(\langle\alpha_\mu^\dagger\alpha_\mu\rangle - \frac{1}{2}\right) \\ &= E_0 + \sum_\mu \epsilon_\mu n_\mu, \end{aligned} \tag{18}$$

where $E_0 = -\frac{1}{2}\sum_{\epsilon_\mu>0}\epsilon_\mu$ is the energy of the ground state and different configurations of n_μ generate 2^N eigenenergies of the spin chain system.

To arrive at our final destination of observing the DTC in this periodically driven spin chain, we first concentrate on the evolution of operator $\hat{\alpha}_\mu^\dagger$,

$$\hat{\alpha}_\mu^\dagger(nT) = \hat{U}_T^{-n}\hat{\alpha}_\mu^\dagger(0)\hat{U}_T^n = \hat{\alpha}_\mu^\dagger(0)e^{inT\epsilon_\mu}. \tag{19}$$

For a given initial state, the expectation value of the operator $\hat{\alpha}_\mu^\dagger$ oscillates with period $2\pi/\epsilon_\mu$. Generally, this oscillating behavior is not rigid and easily perturbed, so the performance for operators $\hat{\alpha}_\mu^\dagger(nT)$ cannot be regarded as a signal of the DTC phase. However, there is an exception due to anomalous edge states in Floquet topological systems. As is shown in Fig. 1(c), such systems exhibit two kinds of edge states with eigenenergies $\epsilon_\mu = 0$ and $\epsilon_\mu = \pi/T$, protected by topological invariants ν_0 and ν_π, respectively. Here, we mainly focus on the edge states with eigenenergy $\epsilon_\mu = \pi/T$, denoted as $H_{\text{eff}}|W\rangle = \pi/T|W\rangle$, and we define $\hat{\beta}_\pi^\dagger = \hat{\Psi}^\dagger|W\rangle$. As shown in Fig 1(d), for an eigenstate $|E\rangle$ with eigenenergy E, $\hat{\beta}_\pi^\dagger$ creates a quasiparticle with quasienergy $\epsilon_\mu = \pi/T$ and excites $|E\rangle$ to another eigenstate $|E + \pi/T\rangle$. Therefore, when $\epsilon_\mu = \pi/T$ exists the eigenenergy of $\hat{H}_{\text{eff}}$ eigenstate $|E\rangle$ and $|E + \pi/T\rangle$ must come in a pair, which leads to the DTC oscillation of some specific observables. As is derived in Eq. (19), the expectation value of the operator $\hat{\beta}_\pi^\dagger$ exactly oscillates with period $2T$. More importantly, this oscillation period is protected by the Floquet topologically nontrivial phases such that this phenomenon of the DTC is robust against symmetry-preserving perturbations. Some previous papers also discuss the relation between the energy spectrum and generating operators $\hat{\beta}_\pi^\dagger$ [19,36,37] and the stability of the boundary discrete time crystal [38].

To further demonstrate the DTC induced by Floquet topological superconductors, we systematically discuss the phase diagrams of Floquet topological superconductors in Sec. III and discuss the DTC for different observables, including anomalous edge operators and end spin operators, in Sec. IV.

III. FLOQUET TOPOLOGICAL PHASES

Following the standard approach of studying topological superconductors, we calculate the topological invariants of the effective Hamiltonian in momentum space. $\hat{H}_{\text{eff}}$ is expressed as

$$\hat{H}_{\text{eff}} = \sum_k (\hat{\gamma}_{k,1} \quad \hat{\gamma}_{k,2}) H_{\text{eff}}(k)\begin{pmatrix}\hat{\gamma}_{k,1}\\ \hat{\gamma}_{k,2}\end{pmatrix}, \tag{20}$$

where $H_{\rm eff}(k)$ are obtained from

$$U(k) = \exp[-iH_2(k)t_2]\exp[-iH_1(k)t_1] = \exp[-iH_{\rm eff}(k)T] \tag{21}$$

according to Appendix A. Here, $d^0_{\rm eff}(k)$ and $\boldsymbol{d}_{\rm eff}(k)$ are defined using $H_{\rm eff}(k) = d^0_{\rm eff}(k)I + \boldsymbol{d}_{\rm eff}(k)\cdot\boldsymbol{\sigma}$. In the following, we request $\epsilon(k) = d^0_{\rm eff}(k) \pm \sqrt{d^2_{\rm eff}(k)} \neq 0$ or π/T for any $k \in [-\pi, \pi)$, due to that the topological superconductors should be gapped.

For a one-dimensional two-band system with intrinsic particle-hole constraint, topologically nontrivial phases can only be classified into classes BDI (with chiral symmetry) and D (without chiral symmetry) [50,51]. So, in the following, we discuss the calculations of topological invariants for classes D and BDI, respectively.

A. D class

For simplicity, we take $J^{yy}_1 = J^{yy}_2 = 0, J^{xx}_2 = h^z_1 = 0$, and nonzero coupling strengths $J^{xy}_1 = J^{xy}_2 = J^{yx}_1 = J^{yx}_2$ to break chiral symmetry. Besides, here and after, we take $t_1 = t_2 = T/2$. Then $H_1(k)$ and $H_2(k)$ are given by

$$\begin{aligned} H_1(k) &= -J^{xx}_1[\sin(k)\sigma_x - \cos(k)\sigma_y] + \left(J^{xy}_1 + J^{yx}_1\right)\sin(k)\sigma_z, \\ H_2(k) &= h^z_2\sigma_y + \left(J^{xy}_1 + J^{yx}_1\right)\sin(k)\sigma_z. \end{aligned} \tag{22}$$

Following the approach in Ref. [52], topological invariants ν_0 and ν_π in Floquet superconductors have such forms

$$\begin{aligned} \nu_0\nu_\pi &= \mathrm{sgn}\,[\mathrm{Pf}(M_0)]\,\mathrm{sgn}\,[\mathrm{Pf}(M_\pi)], \\ \nu_0 &= \mathrm{sgn}\,[\mathrm{Pf}(N_0)]\,\mathrm{sgn}\,[\mathrm{Pf}(N_\pi)], \end{aligned} \tag{23}$$

where $\mathrm{Pf}[X]$ is the Pfaffian number of a skew matrix X and $M_k = \ln[U(k)]$, $N_k = \ln[\sqrt{U(k)}]$. Since both $\ln(X)$ and $\ln(\sqrt{X})$ are multivalued functions, for $k = 0$ and $k = \pi$ we have

$$M_k = -i\xi_M(k)\sigma_y, \quad N_k = -i\xi_N(k)\sigma_y, \tag{24}$$

with

$$\begin{aligned} \xi_M(k) + 2z\pi &= J^{xx}_1 t\cos(k) + h^z_2 t, \\ \xi_N(k) + 2z\pi &= \frac{J^{xx}_1 t\cos(k) + h^z_2 t}{2}. \end{aligned} \tag{25}$$

Here, z is taken as an appropriate integer so that $\xi_{M/N}(k)$ can be constrained to the interval $[-\pi, \pi)$. Finally, we obtain

$$\begin{aligned} \nu_0\nu_\pi &= \mathrm{sgn}[\sin(P_+)\sin(P_-)], \\ \nu_0 &= \mathrm{sgn}\left[\sin\left(\frac{P_+}{2}\right)\sin\left(\frac{P_-}{2}\right)\right], \end{aligned} \tag{26}$$

with

$$\begin{aligned} P_+ &= h^z_2 t + J^{xx}_1 t, \\ P_- &= h^z_2 t - J^{xx}_1 t. \end{aligned} \tag{27}$$

In Figs. 2(a) and 2(b), we show the phase diagrams of topological invariants ν_0 and ν_π on the θ_1-θ_2 plane by taking $\theta_1 = J^{xx}_1 t$ and $\theta_2 = h^z_2 t$. For the D class, the system is classified by a $\mathbb{Z}_2$ topological invariant. ν_0 and ν_π take the value ± 1, and $\nu_\pi = -1$ indicates anomalous topologically nontrivial phases. The quasienergy spectrum as a function of

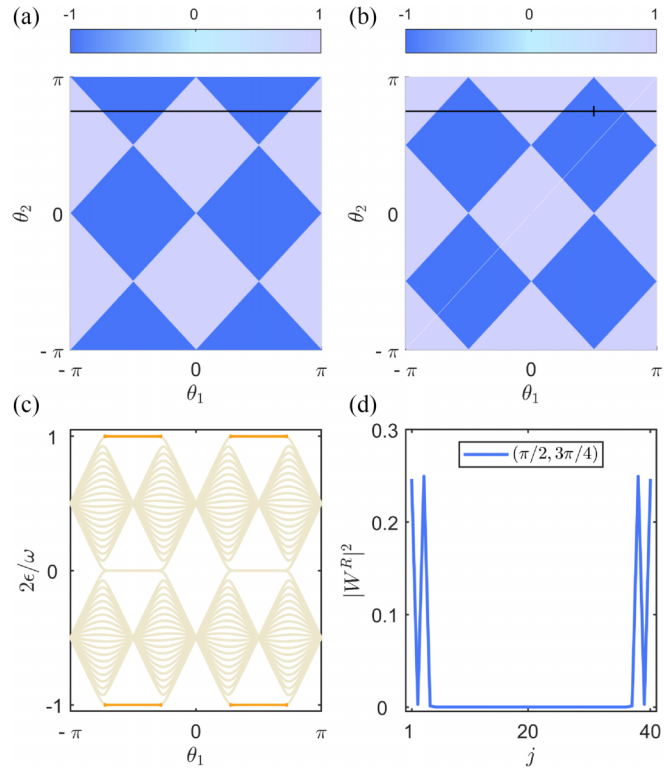

FIG. 2. (a), (b) Phase diagrams of the D class topological superconductor (without chiral symmetry). The areas of topological invariants with value -1 indicate a topologically nontrivial superconductor, otherwise topologically trivial. Topological invariant ν_0 is shown in (a) and ν_π in (b). (c) Quasienergy spectrum of the topological superconductor under open boundary condition with parameters $\theta_1 \in [-\pi, \pi)$, $\theta_2 = 3\pi/4$ along the black solid line shown in (a), (b). (d) π-mode edge state $|W^R\rangle$ with parameters $(\theta_1, \theta_2) = (\pi/2, 3\pi/4)$. Here, we set $J^{xx}_1 T/2 = \theta_1, h^z_2 T/2 = \theta_2$.

$\theta_1 \in [-\pi, \pi)$ is plotted in Fig. 2(c). The gapless 0 mode and π mode must exist where the topological invariants $\nu_0 = -1$ and $\nu_\pi = -1$, respectively. Consequently, the topologically protected discrete time crystal could be observed in the regime $\nu_\pi = -1$.

Furthermore, because of particle-hole symmetry, the eigenvalues and eigenvectors of $H_{\rm eff}$ always come in pairs as shown in Eq. (16). Thus for the edge states with quasienergies $\epsilon_\mu = 0$ or π/T, the eigenvectors $|V_\mu\rangle$ and $|V^*_\mu\rangle$ span a degenerate subspace, from which we can construct a pure real vector and a pure imaginary vector as $|V^R_\mu\rangle = |V_\mu\rangle + |V^*_\mu\rangle$ and $|V^I_\mu\rangle = |V_\mu\rangle - |V^*_\mu\rangle$. In Fig. 2(d), we have shown the probability distribution of an anomalous edge state $|W^R\rangle = (|W\rangle + |W^*\rangle)/\sqrt{2}$. For convenience, here and after, $\{j, s\}$ $(j = 1, 2, \ldots, L$ and $s = 1, 2)$ in Eq. (7) is relabeled as $\{2j + s - 2\}$ for the index of $\hat{\gamma}$, as well as $|W^R\rangle$.

B. BDI class

For simplicity, we take nonzero coupling strengths $J^{xx}_1 = J^{xx}_2$, h^z_2 and other parameters zero so that the system obeys chiral symmetry. With given parameters, the chiral operator is

taken as $U_S = \sigma_z$ and we have

$$U_S^\dagger U^{a,b} U_S = (U^{a,b})^\dagger, \tag{28}$$

where

$$\begin{aligned} U^a &= \exp(-iH_1 t_1/2)\exp(-iH_2 t_2)\exp(-iH_1 t_1/2) \\ &= \exp(-iH_{\text{eff}}^a T), \\ U^b &= \exp(-iH_2 t_2/2)\exp(-iH_1 t_1)\exp(-iH_2 t_2/2) \\ &= \exp(-iH_{\text{eff}}^b T), \end{aligned} \tag{29}$$

and

$$\begin{aligned} H_1(k) &= -J_1^{xx}[\sin(k)\sigma_x - \cos(k)\sigma_y], \\ H_2(k) &= h_2^z \sigma_y - J_1^{xx}[\sin(k)\sigma_x - \cos(k)\sigma_y]. \end{aligned} \tag{30}$$

Here, we introduce U^a and U^b, which are both unitarily transformed from $U(k)$, in order that the chiral operator is explicitly σ_z. Besides, based on U^a and U^b the topological invariants ν_0 and ν_π can be calculated as [53,54] follows,

$$\nu_{0,\pi} = \frac{\nu_a \pm \nu_b}{2}, \tag{31}$$

where ν_a and ν_b are the winding numbers defined as

$$\nu_{a,b} = \frac{1}{2\pi}\int dk \frac{-d_{a,b}^x(k)\partial_k d_{a,b}^y(k) + d_{a,b}^y(k)\partial_k d_{a,b}^x(k)}{\left[d_{a,b}^x(k)\right]^2 + \left[d_{a,b}^y(k)\right]^2}, \tag{32}$$

and $d_{a,b}^{x,y}(k)$ is given by

$$H_{\text{eff}}^{a,b}(k) = d_{a,b}^x(k)\sigma_x + d_{a,b}^y(k)\sigma_y. \tag{33}$$

In Figs. 3(a) and 3(b), we show the phase diagrams of topological invariants ν_0 and ν_π on the θ_1-θ_2 plane. For the BDI class, the system is classified by a $\mathbb{Z}$ topological invariant. Both ν_0 and ν_π take integer values, and $\nu_\pi \neq 0$ indicates anomalous topologically nontrivial phases. The quasienergy spectrum as a function of $\theta_1 \in [-\pi, \pi)$ is plotted in Fig. 2(c). In contrast to the D class, the topological invariant in class BDI ν_0 and ν_π could be $\pm 2, \pm 3, \ldots$ leading to larger degeneracy of edge states. For example, for $(\theta_1, \theta_2) = (3\pi/8, 7\pi/8)$, we have $\nu_\pi = 2$, which results in four π-mode edge states. These four edge states are labeled as $|W_\eta\rangle$ and $|W_\eta^*\rangle$ with $\eta = 1, 2$. In Fig. 3(d), we show the probability distribution of the anomalous edge states as $|W_{\eta=1}^R\rangle$ and $|W_{\eta=2}^R\rangle$, respectively.

Here, we remark that when parameters in our scheme are taken as $J_{1,2}^{xy} = J_{1,2}^{yx} = J_{1,2}^{yy} = J_2^{xx} = h_1^z = 0$, the setup is reduced to the situation discussed in Ref. [19]. The topologically nontrivial phases with $\nu_0 = \nu_\pi = 1$ and $\nu_0 = 0, \nu_\pi = 1$ correspond to "0π-PM phase" and "π-SG phase," respectively, which have been discussed a great deal previously [19,36–38].

IV. SUBHARMONIC OSCILLATIONS OF THE DTC

In this section, we will examine the subharmonic oscillations of the DTC in topologically nontrivial phases with $\nu_\pi = -1$ in the D class and $\nu_\pi \neq 0$ in the BDI class, by selecting the anomalous edge mode and the end spin as observables.

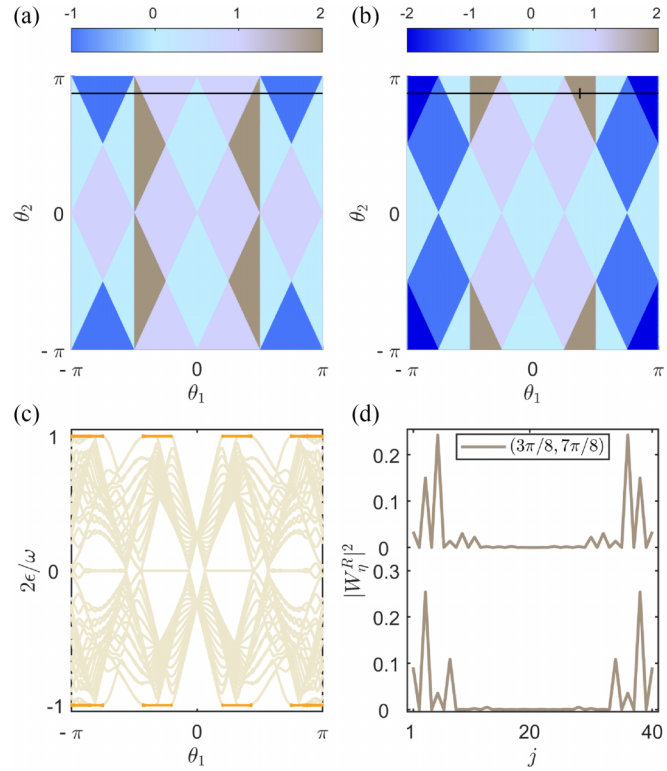

FIG. 3. (a), (b) Phase diagrams of the BDI class topological superconductor (with chiral symmetry). The areas of topological invariants with nonzero values indicate a topologically nontrivial superconductor, otherwise topologically trivial. Topological invariant ν_0 is shown in (a) and ν_π in (b). (c) Quasienergy spectrum of the topological superconductor under open boundary condition with parameters $\theta_1 \in [-\pi, \pi)$, $\theta_2 = 7\pi/8$ along the black solid line shown in (a), (b). (d) π-mode edge state $|W^R\rangle$ with parameters $(\theta_1, \theta_2) = (3\pi/8, 7\pi/8)$. Here, we set $\theta_1 = J_1^{xx}T/2 = J_2^{xx}T/2$, $\theta_2 = h_2^z T/2$.

We first take the anomalous edge mode as the observable for the DTC,

$$\hat{\beta}_\pi^R = \frac{\hat{\beta}_\pi + \hat{\beta}_\pi^\dagger}{\sqrt{2}}. \tag{34}$$

As we have derived in Eq. (19), the time evolution of observable $\hat{\beta}_\pi^R$ is expressed as

$$\begin{aligned} \langle \hat{\beta}_\pi^R(nT)\rangle &= \langle \psi(0)|\hat{U}_T^{-n}\hat{\beta}_\pi^R\hat{U}_T^n|\psi(0)\rangle \\ &= (-1)^n\langle\psi(0)|\hat{\beta}_\pi^R|\psi(0)\rangle. \end{aligned} \tag{35}$$

It is obvious that the dynamics of $\langle\hat{\beta}_\pi^R(nT)\rangle$ manifests an exact subharmonic response for a generic initial state with $\langle\psi(0)|\hat{\beta}_\pi^R|\psi(0)\rangle \neq 0$. After the Fourier transformation of $\langle\hat{\beta}_\pi^R(nT)\rangle$, we obtain the response function

$$A_\beta(\omega) = \frac{1}{n_{\max}}\sum_{n=1}^{n_{\max}}\langle\hat{\beta}_\pi^R(nT)\rangle e^{i\omega nT}, \tag{36}$$

where $n_{\max}$ represents the maximal number of periods. In Figs. 4(a) and 4(b), we show the expectation values of $\hat{\beta}_\pi^R$ as a function of evolution time for the D class and BDI class, respectively. Correspondingly the response functions $A_\beta(\omega)$ are plotted in Figs. 4(c) and 4(d). $\langle\hat{\beta}_\pi^R\rangle$ oscillates with double

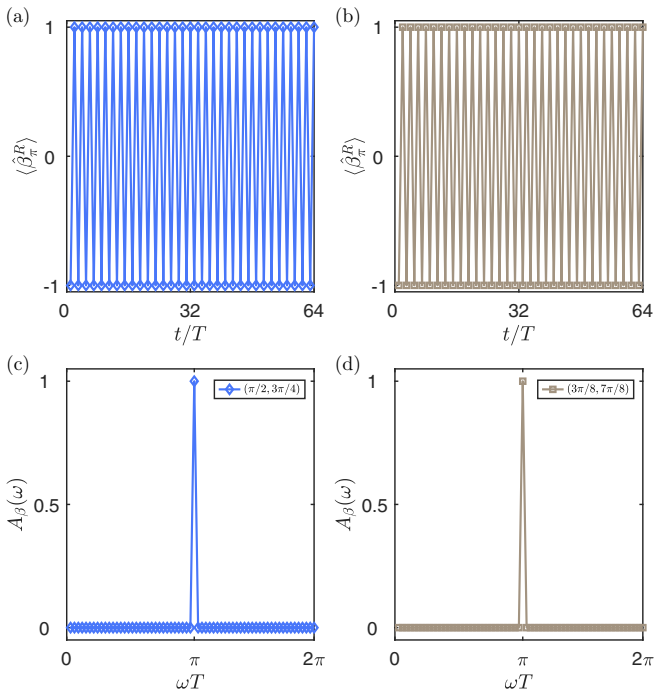

FIG. 4. (a), (b) Dynamics of anomalous edge mode $\hat{\beta}_\pi^R$. (c), (d) Distribution of response function $A_\beta(\omega)$. The frequency distributions in (c) and (d) are the Fourier transformation of dynamics in (a) and (b), respectively. (a), (c) with the same parameters as Fig. 2(d) correspond to D class, while (b), (d) with the same parameters as Fig. 3(d) correspond to BDI class. The initial state is taken as a product state polarized along x direction.

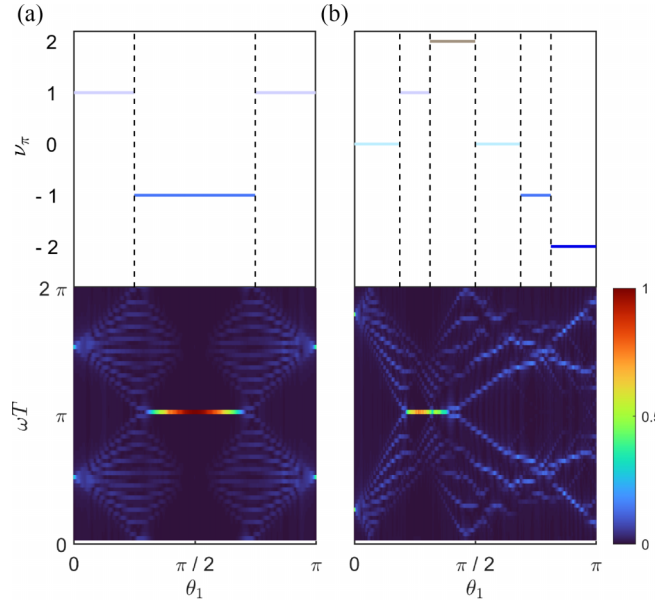

FIG. 5. (a), (b) Upper panels: The values of topological invariants in different regimes. Lower panels: Frequency distributions of the response function for observable $\hat{X}_1$ and the color represents the amplitude of $A_X(\omega)$. Parameters of (a) are the same as the black solid line in Fig. 2, while parameters of (b) are the same as the black solid line in Fig. 3.

periods and $A_\beta(\omega)$ peaks at $\omega = \pi/T$, which confirm the subharmonic response for the observable $\hat{\beta}_\pi^R$ in the regime of Floquet topologically nontrivial phases with anomalous edge states. However, we have to admit that $\hat{\beta}_\pi^R$ is difficult to engineer and observe in experiments, and the concrete form of operator $\hat{\beta}_\pi^R$ in the spin basis depends on coupling parameters. Therefore, it is important to choose a more appropriate operator that is easily observed in experiments.

Another observable for the DTC is taken as the end spin operator $\hat{X}_1$, since the anomalous edge states finitely occupy the end sites. Actually, the end spin $\hat{X}_1$ is nothing but $\hat{\gamma}_1$ after the Jordan-Wigner transformation, which could be decomposed as

$$\hat{\gamma}_1 = \sum_{\eta=1}^{n_{\text{edge}}} |W_\eta\rangle_1 \hat{\beta}_{\pi,\eta} + \sum_{\epsilon_\mu \neq \pi/T} |V_\mu\rangle_1 \hat{\alpha}_\mu + \text{H.c.}, \tag{37}$$

where $|W_\eta\rangle_1$ and $|V_\mu\rangle_1$ represent the first element of vectors $|W_\eta\rangle$ and $|V_\mu\rangle$, respectively. n_{edge} represents the number of pairs of edge states. The dynamics of the observable $\hat{X}_1$ are then given by

$$\begin{aligned}\langle\hat{X}_1(nT)\rangle &= \langle\psi(0)|\hat{U}_T^{-n}\hat{\gamma}_1\hat{U}_T^n|\psi(0)\rangle \\ &= (-1)^n \sum_{\eta=1}^{n_{\text{edge}}} 2\text{Re}[|W_\eta\rangle_1\langle\psi(0)|\hat{\beta}_{\pi,\eta}|\psi(0)\rangle] \\ &\quad + \sum_{\epsilon_\mu\neq\pi/T} 2\text{Re}[|V_\mu\rangle_1 e^{2i\epsilon_\mu}\langle\psi(0)|\hat{\alpha}_\mu|\psi(0)\rangle]. \end{aligned} \tag{38}$$

In the D class, there is only one pair of edge states with $n_{\text{edge}} = 1$, which is localized around $\hat{\gamma}_1|0\rangle$ and $\hat{\gamma}_{2N}|0\rangle$. Therefore, $|W_1\rangle_1$ is finitely distributed so that $\langle\hat{X}_1(nT)\rangle$ manifests a subharmonic response at $\omega = \pi/T$ as is shown in the second line of Eq. (38). In Fig. 5(a), we show the response function $A_X(\omega)$ of $\hat{X}_1$, which peaks at $\omega = \pi/T$ when $\nu_\pi = -1$. These numerical results indicate the presence of the DTC for the end spin observable. But in the BDI class, according to the bulk-edge correspondence [54], $n_{\text{edge}} = |\nu_\pi|$ with $\nu_\pi > 0$ ($\nu_\pi < 0$) represents the number of edge states occupying $\hat{\gamma}_1|0\rangle$ ($\hat{\gamma}_2|0\rangle$). Therefore, $|W_\eta\rangle_1$ is finite when $\nu_\pi > 0$, while $|W_\eta\rangle_1$ is exactly 0 when $\nu_\pi < 0$. As shown in Fig. 5(b), $A(\omega)$ peaks at $\omega = \pi/T$ when $\nu_\pi > 0$, which also indicates the presence of the DTC for the BDI class. Besides, we check the dynamics of the bulk spin in Appendix C, which confirms only that the end spin operator shows the subharmonic oscillations. Note that the DTC regime, where $A(\omega)$ peaks at $\omega = \pi/T$, does not exactly match with the topological region with $\nu_\pi = -1$ ($\nu_\pi > 0$) for the D (BDI) class. We think this phenomenon is due to the finite-size effect, which causes the quasienergy of the edge mode to be not perfectly π/T. In order to check the finite-size effect, the numerical results for different lengths of the chain are shown in Appendix B.

V. ROBUSTNESS OF THE DTC

In order to demonstrate the robustness of the DTC induced by topological superconductors, we continue to investigate the frequency distributions of response function for $\hat{X}_1$ after adding symmetry-preserving and symmetry-breaking perturbations.

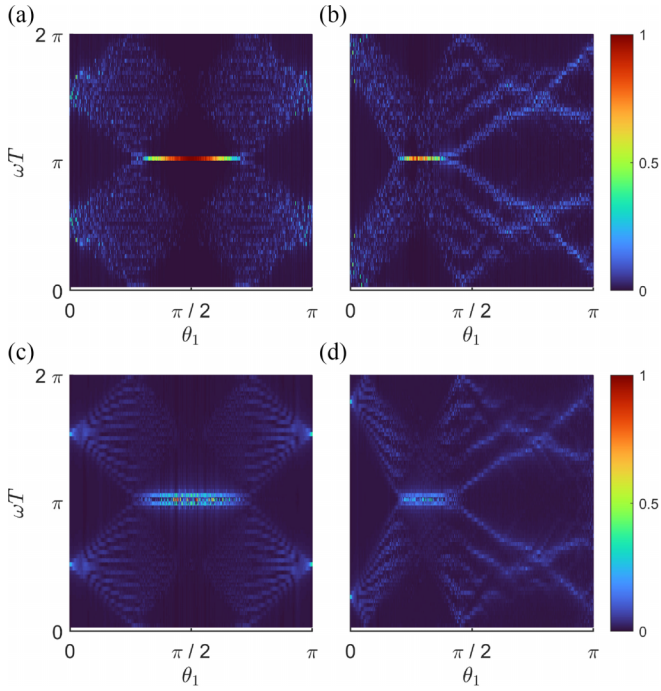

FIG. 6. (a)–(d) Frequency distributions of the response function for observable $\hat{X}_1$ and the color represents the amplitude of $A_X(\omega)$. In (a) and (b), $\sum_j \delta_j \hat{Z}_j$ is added which preserves the particle-hole symmetry, while in (c) and (d) $\sum_j \delta_j \hat{X}_j$ is added which breaks the particle-hole symmetry. Parameters of (a), (c) are the same as the black solid line in Fig. 2, while parameters of (b), (d) are the same as the black solid line in Fig. 3. δ_j is randomly distributed in $[-0.1h_2^z, 0.1h_2^z]$, which is only added in the second interval during a period.

For the D class or BDI class, the Hamiltonian obeys particle-hole symmetry, which means the Hamiltonian (4) is invariant after particle-hole transformation $\hat{c}_j^\dagger \to (-1)^j \hat{c}_j$, $\hat{c}_j \to (-1)^j \hat{c}_j^\dagger$, and $i \to -i$. In the following, we add an operator $\sum_j \delta_j \hat{Z}_j$ as the particle-hole symmetry-preserving perturbation and $\sum \delta_j \hat{X}_j$ as the symmetry-breaking perturbation, with δ_j disordered parameters. As shown in Figs. 6(a) and 6(b), the frequency distributions of Eq. (36), for the D class and BDI class, respectively, are almost unaffected by the symmetry-preserving perturbation. As a comparison, the subharmonic response is collapsed after adding symmetry-breaking perturbations for both classes. These results suggest that subharmonic response is robust to symmetry-preserving perturbations, which confirms the DTC is originated from topologically nontrivial phases.

VI. SUMMARY

We have systematically studied the Floquet time crystal in a periodically driven spin chain model by elaborating the topological classifications and phase diagrams after mapping it to a Majorana chain. In this paper, we have shown that the dynamics of the observable edge mode operator or end spin operator indeed exhibit robust subharmonic oscillation, which is a typical signature of the DTC. Besides, the rigidity and robustness of the DTC build on the topologically nontrivial phase, as well as solvability, which prevents the systems from

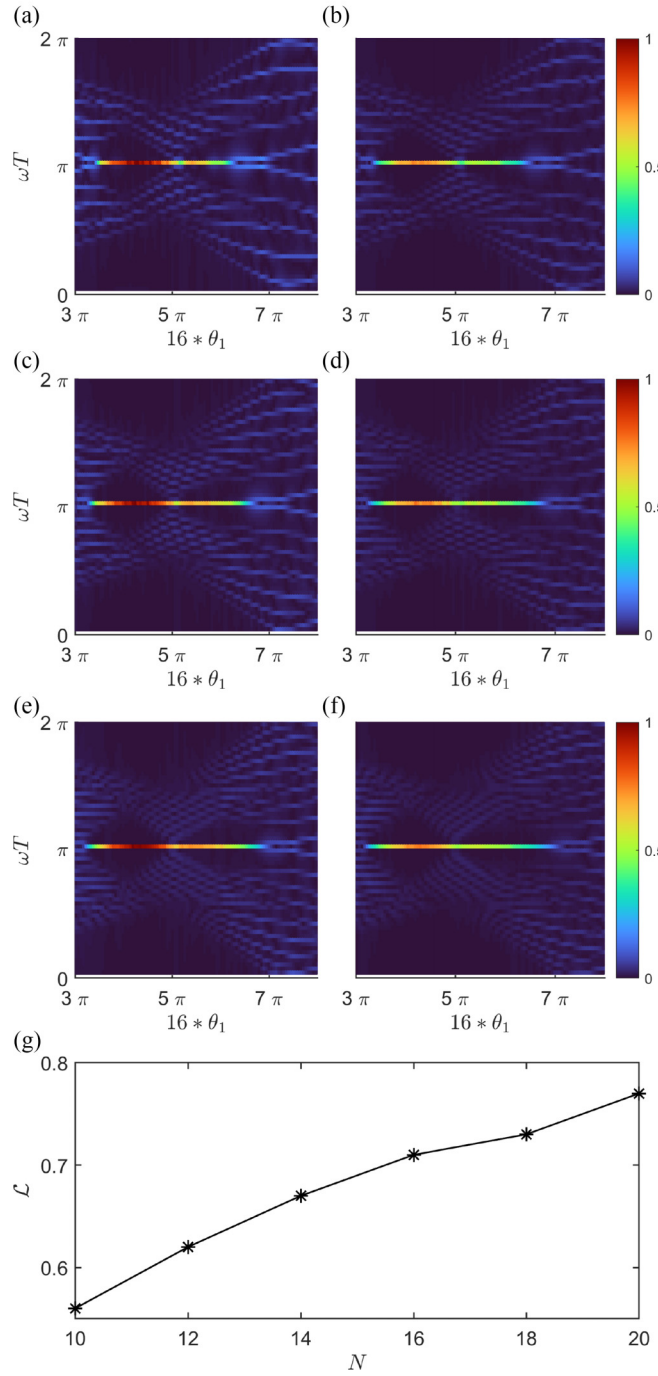

FIG. 7. (a)–(f) Frequency distributions of the response function for observable $\hat{X}_1$ and the color represents the amplitude of $A_X(\omega)$. The length of chain N increases from 10 to 12, 14, 16, 18, 20, corresponding to (a)–(f), respectively. Parameters are the same as Fig. 5 except for $\theta_1 \in [3\pi/16, \pi/2]$, which is the topologically nontrivial regime with $\nu_\pi \neq 0$. (g) The regime of parameter θ_1 satisfying $A_X(\omega = \pi/T) > 0.05$ varies with the length of chain N.

thermalization. Furthermore, since the system is a general spin chain model and can be strictly solved, it is potentially generalized to other interacting or dissipative systems. Our results might be helpful in deeply understanding the mechanism for other kinds of DTC. Besides, the model is easily implemented

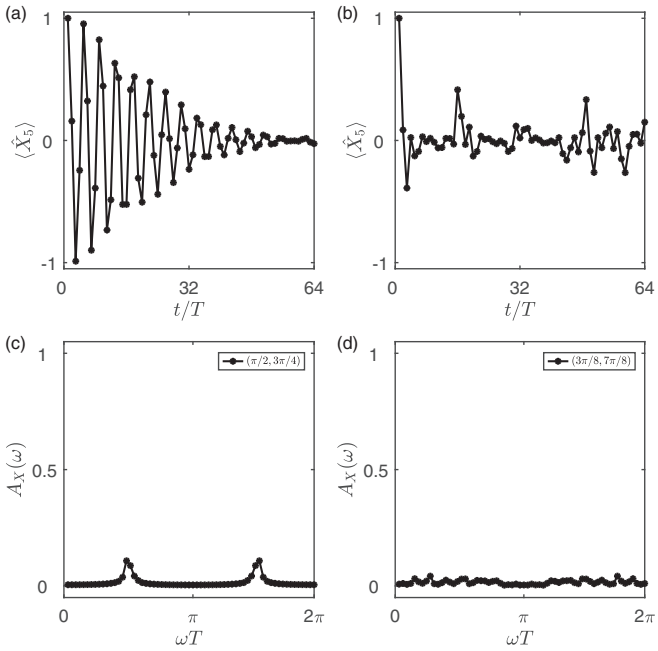

FIG. 8. (a), (b) Dynamics of $\langle \hat{X}_5 \rangle$. (c), (d) Distribution of response function $A_X(\omega)$. The frequency distributions in (c) and (d) are the Fourier transformation of dynamics in (a) and (b), respectively. (a), (c) with the same parameters as Fig. 2(d) in the main text correspond to D class, while (b), (d) with the same parameters as Fig. 3(d) in the main text correspond to BDI class. The initial state is taken as a product state polarized along x direction.

and the topological DTC for the end spin is readily realized in experiments.

ACKNOWLEDGMENTS

We would like to thank Hui Zhai, Wei Zheng, Chengshu Li, Yanting Cheng, Haifeng Tang, and Fan Yang for helpful discussions. This work has been supported by the National Natural Science Foundation of China (Grant No. 12204428).

APPENDIX A: PROOF OF EQUATION (8)

In this Appendix, we prove that the effective Hamiltonian $\hat{H}_{\text{eff}}$, defined by

$$\exp(-i\hat{H}_{\text{eff}}T) = \exp(-i\hat{H}_2 t_2)\exp(-i\hat{H}_1 t_1), \tag{A1}$$

is quadratic with $\hat{H}_{\text{eff}} = \frac{1}{2}\hat{\Psi}^\dagger H_{\text{eff}}\hat{\Psi}$, where H_{eff} has such form

$$\exp(-iH_{\text{eff}}T) = \exp(-iH_2 t_2)\exp(-iH_1 t_1). \tag{A2}$$

First, we rewrite $\hat{H}_{\text{eff}}$ by means of the Baker-Campbell-Hausdorff formula as

$$\hat{H}_{\text{eff}} = \frac{1}{T}\Big\{\hat{H}_1 t_1 + \hat{H}_2 t_2 - \frac{it_1t_2}{2}[\hat{H}_1, \hat{H}_2] - \frac{t_1^2 t_2}{12}[\hat{H}_1, [\hat{H}_1, \hat{H}_2]] - \frac{t_1 t_2^2}{12}[\hat{H}_2, [\hat{H}_2, \hat{H}_1]]\ldots\Big\}. \tag{A3}$$

Second, since the right-hand side of Eq. (A3) is made up of a series of commutators, we choose $[\hat{H}_1, \hat{H}_2]$ as a typical term to analyze. Because both $\hat{H}_1$ and $\hat{H}_2$ have the quadratic form as $\hat{H}_m = \frac{1}{2}\hat{\Psi}^\dagger H_m \hat{\Psi}$, we define a mapping from a matrix to an operator as $\hat{\Gamma}(H_m) = \frac{1}{2}\sum_{i,j}(H_m)_{i,j}\gamma_i\gamma_j$.

Third, we prove the relation $\hat{\Gamma}([H_1, H_2]) = [\hat{\Gamma}(H_1), \hat{\Gamma}(H_2)]$ in the following process,

$$\begin{aligned}
[\hat{H}_1, \hat{H}_2] &= \frac{1}{4}\sum_{ij}\sum_{u,v}(H_1)_{i,j}(H_2)_{u,v}(\gamma_i\gamma_j\gamma_u\gamma_v - \gamma_u\gamma_v\gamma_i\gamma_j) \\
&= \frac{1}{4}\sum_{i,j}\sum_{u,v}(H_1)_{i,j}(H_2)_{u,v}\gamma_i(\delta_{u,j} - \gamma_u\gamma_j)\gamma_v - \frac{1}{4}\sum_{i,j}\sum_{u,v}(H_1)_{i,j}(H_2)_{u,v}\gamma_u(\delta_{v,i} - \gamma_i\gamma_v)\gamma_j \\
&= \frac{1}{4}\sum_{i,j}\sum_{u,v}(H_1)_{i,j}(H_2)_{u,v}\delta_{u,j}\gamma_i\gamma_v - \frac{1}{4}\sum_{i,j}\sum_{u,v}(H_2)_{u,v}(H_1)_{i,j}\delta_{v,i}\gamma_u\gamma_j \\
&\quad - \frac{1}{4}\sum_{i,j}\sum_{u,v}(H_1)_{i,j}(H_2)_{u,v}(\delta_{u,i} - \gamma_u\gamma_i)\gamma_j\gamma_v + \frac{1}{4}\sum_{i,j}\sum_{u,v}(H_1)_{i,j}(H_2)_{u,v}\gamma_u\gamma_i(\delta_{v,j} - \gamma_j\gamma_v) \\
&= \frac{1}{2}(H_1H_2 - H_2H_1)_{i,j}\gamma_i\gamma_j \\
&= \hat{\Gamma}([H_1, H_2]),
\end{aligned} \tag{A4}$$

where we have used the property that matrices H_1 and H_2 are both antisymmetric. Using the relation of Eq. (A4), we can prove $[\hat{H}_1, [\hat{H}_1, \hat{H}_2]] = \hat{\Gamma}([H_1, [H_1, H_2]])$, $[\hat{H}_2, [\hat{H}_2, \hat{H}_1]] = \hat{\Gamma}([H_2, [H_1, H_2]])$, and so on. In this way, every term in Eq. (A3) can be rewritten as the quadratic form $\hat{\Gamma}$, so we have $\hat{H}_{\text{eff}} = \hat{\Gamma}(H_{\text{eff}})$, where

$$H_{\text{eff}} = \frac{1}{T}\Big\{H_1 t_1 + \hat{H}_2 t_2 - \frac{it_1t_2}{2}[H_1, H_2] - \frac{t_1^2 t_2}{12}[H_1, [H_1, H_2]] - \frac{t_1 t_2^2}{12}[H_2, [H_2, H_1]]\ldots\Big\}. \tag{A5}$$

Again, we use the Baker-Campbell-Hausdorff formula and H_{eff} is obtained according to $\exp(-iH_{\text{eff}}T) = \exp(-iH_1t_1)\exp(-iH_2t_2)$.

APPENDIX B: FINITE-SIZE EFFECT

In Fig. 5, the DTC regime, where $A_X(\omega)$ peaks at $\omega = \pi/T$, is smaller than the region of topologically nontrivial phases. We think this phenomenon is due to the finite-size effect, which causes the quasienergy of anomalous edge state to be not perfectly π/T. As an example, we numerically calculate the DTC regimes for the BDI class as the length of chain N increases to show the finite-size effect. The numerical results are shown in Fig. 7, from which we find that the regime of parameter θ_1 satisfying $A_X(\omega = \pi/T) > 0.05$ increases as the length of chain increases. It is inferred that the regime of parameter θ_1 could match with the region of topologically nontrivial phases as $N \to \infty$.

APPENDIX C: DYNAMICS OF BULK SPINS

In order to confirm that only the end spin shows the subharmonic oscillations, while the bulk spin does not show this behavior, we numerically calculate the dynamics of a typical bulk spin $\langle \hat{X}_5 \rangle$ in the D class and BDI class. The numerical results are shown in Fig. 8. According to the dynamics and frequency distributions in this figure, we find that the bulk spin indeed does not show the subharmonic oscillations. These results demonstrate that the DTC behavior, which originates from topological edge states, only exists around the boundary of the spin chain.

[1] A. Zenesini, H. Lignier, D. Ciampini, O. Morsch, and E. Arimondo, Phys. Rev. Lett. **102**, 100403 (2009).
[2] P. Xu, T.-S. Deng, W. Zheng, and H. Zhai, Phys. Rev. A **103**, L061302 (2021).
[3] L. W. Clark, B. M. Anderson, L. Feng, A. Gaj, K. Levin, and C. Chin, Phys. Rev. Lett. **121**, 030402 (2018).
[4] Y.-Y. Chen, P. Zhang, W. Zheng, Z. Wu, and H. Zhai, Phys. Rev. A **102**, 011301 (2020).
[5] C. Lv, R. Zhang, and Q. Zhou, Phys. Rev. Lett. **125**, 253002 (2020).
[6] G. Jotzu, M. Messer, R. Desbuquois, M. Lebrat, T. Uehlinger, D. Greif, and T. Esslinger, Nature (London) **515**, 237 (2014).
[7] M. Aidelsburger, M. Lohse, C. Schweizer, M. Atala, J. T. Barreiro, S. Nascimbène, N. Cooper, I. Bloch, and N. Goldman, Nat. Phys. **11**, 162 (2015).
[8] J. Zhang, P. W. Hess, A. Kyprianidis, P. Becker, A. Lee, J. Smith, G. Pagano, I.-D. Potirniche, A. C. Potter, A. Vishwanath *et al.*, Nature (London) **543**, 217 (2017).
[9] S. Choi, J. Choi, R. Landig, G. Kucsko, H. Zhou, J. Isoya, F. Jelezko, S. Onoda, H. Sumiya, V. Khemani *et al.*, Nature (London) **543**, 221 (2017).
[10] J. Rovny, R. L. Blum, and S. E. Barrett, Phys. Rev. Lett. **120**, 180603 (2018).
[11] S. Pal, N. Nishad, T. S. Mahesh, and G. J. Sreejith, Phys. Rev. Lett. **120**, 180602 (2018).
[12] H. Keßler, P. Kongkhambut, C. Georges, L. Mathey, J. G. Cosme, and A. Hemmerich, Phys. Rev. Lett. **127**, 043602 (2021).
[13] J. Randall, C. Bradley, F. van der Gronden, A. Galicia, M. Abobeih, M. Markham, D. Twitchen, F. Machado, N. Yao, and T. H. Taminiau, Science **374**, 1474 (2021).
[14] A. Kyprianidis, F. Machado, W. Morong, P. Becker, K. Collins, D. Else, L. Feng, P. Hess, C. Nayak, G. Pagano, N. Yao, and C. Monroe, Science **372**, 1192 (2021).
[15] D. Bluvstein, A. Omran, H. Levine, A. Keesling, G. Semeghini, S. Ebadi, T. Wang, A. Michailidis, N. Maskara, W. W. Ho *et al.*, Science **371**, 1355 (2021).
[16] X. Mi, M. Ippoliti, C. Quintana, A. Greene, Z. Chen, J. Gross, F. Arute, K. Arya, J. Atalaya, R. Babbush, J. Bardin, J. Basso, A. Bengtsson, A. Bilmes, A. Bourassa, L. Brill, M. Broughton, B. Buckley, D. Buell, and P. Roushan, Nature (London) **601**, 531 (2022).
[17] X. Zhang, W. Jiang, J. Deng, K. Wang, J. Chen, P. Zhang, W. Ren, H. Dong, S. Xu, Y. Gao *et al.*, Nature (London) **607**, 468 (2022).
[18] P. Frey and S. Rachel, Sci. Adv. **8**, eabm7652 (2022).
[19] V. Khemani, A. Lazarides, R. Moessner, and S. L. Sondhi, Phys. Rev. Lett. **116**, 250401 (2016).
[20] D. V. Else, B. Bauer, and C. Nayak, Phys. Rev. Lett. **117**, 090402 (2016).
[21] N. Y. Yao, A. C. Potter, I.-D. Potirniche, and A. Vishwanath, Phys. Rev. Lett. **118**, 030401 (2017).
[22] B. Huang, Y.-H. Wu, and W. V. Liu, Phys. Rev. Lett. **120**, 110603 (2018).
[23] Z. Gong, R. Hamazaki, and M. Ueda, Phys. Rev. Lett. **120**, 040404 (2018).
[24] B. Zhu, J. Marino, N. Y. Yao, M. D. Lukin, and E. A. Demler, New J. Phys. **21**, 073028 (2019).
[25] K. Chinzei and T. N. Ikeda, Phys. Rev. Lett. **125**, 060601 (2020).
[26] B. Huang, T.-H. Leung, D. M. Stamper-Kurn, and W. V. Liu, Phys. Rev. Lett. **129**, 133001 (2022).
[27] F. Wilczek, Phys. Rev. Lett. **109**, 160401 (2012).
[28] P. Bruno, Phys. Rev. Lett. **111**, 070402 (2013).
[29] H. Watanabe and M. Oshikawa, Phys. Rev. Lett. **114**, 251603 (2015).
[30] S. Sarkar and Y. Dubi, Commun. Phys **5**, 155 (2022).
[31] S. Sarkar and Y. Dubi, Nano Lett. **22**, 4445 (2022).
[32] H. Taheri, A. Matsko, L. Maleki, and K. Sacha, Nat. Commun. **13**, 848 (2022).
[33] M. S. Rudner, N. H. Lindner, E. Berg, and M. Levin, Phys. Rev. X **3**, 031005 (2013).
[34] P. Titum, E. Berg, M. S. Rudner, G. Refael, and N. H. Lindner, Phys. Rev. X **6**, 021013 (2016).
[35] L. Zhou and J. Gong, Phys. Rev. B **97**, 245430 (2018).
[36] C. W. von Keyserlingk and S. L. Sondhi, Phys. Rev. B **93**, 245145 (2016).
[37] C. W. von Keyserlingk and S. L. Sondhi, Phys. Rev. B **93**, 245146 (2016).
[38] C. W. von Keyserlingk, V. Khemani, and S. L. Sondhi, Phys. Rev. B **94**, 085112 (2016).

[39] R. W. Bomantara and J. Gong, Phys. Rev. Lett. **120**, 230405 (2018).
[40] Y. Pan and B. Wang, Phys. Rev. Res. **2**, 043239 (2020).
[41] A. Chew, D. F. Mross, and J. Alicea, Phys. Rev. Lett. **124**, 096802 (2020).
[42] O. Shtanko and R. Movassagh, Phys. Rev. Lett. **125**, 086804 (2020).
[43] R. W. Bomantara, S. Mu, and J. Gong, Phys. Rev. B **103**, 235404 (2021).
[44] B. Wang, J. Quan, J. Han, X. Shen, H. Wu, and Y. Pan, Laser Photonics Rev. **16**, 2100469 (2022).
[45] F. Iemini, A. Russomanno, J. Keeling, M. Schirò, M. Dalmonte, and R. Fazio, Phys. Rev. Lett. **121**, 035301 (2018).
[46] G. Piccitto, M. Wauters, F. Nori, and N. Shammah, Phys. Rev. B **104**, 014307 (2021).
[47] L. F. d. Prazeres, L. d. S. Souza, and F. Iemini, Phys. Rev. B **103**, 184308 (2021).
[48] F. Carollo and I. Lesanovsky, Phys. Rev. A **105**, L040202 (2022).
[49] A. C. Lourenço, L. F. d. Prazeres, T. O. Maciel, F. Iemini, and E. I. Duzzioni, Phys. Rev. B **105**, 134422 (2022).
[50] C.-K. Chiu, J. C. Y. Teo, A. P. Schnyder, and S. Ryu, Rev. Mod. Phys. **88**, 035005 (2016).
[51] The BdG constraint requires $C^{-1}HC = -H$ with $C^2 = 1$, which means only classes D, BDI, and DIII are allowed in a 1-D system. However, for class DIII it also requires $T^{-1}HT = -H$ with $T^2 = -1$, which leads to a trivial result for a two-band model.
[52] L. Jiang, T. Kitagawa, J. Alicea, A. R. Akhmerov, D. Pekker, G. Refael, J. I. Cirac, E. Demler, M. D. Lukin, and P. Zoller, Phys. Rev. Lett. **106**, 220402 (2011).
[53] J. K. Asbóth and H. Obuse, Phys. Rev. B **88**, 121406(R) (2013).
[54] J. K. Asbóth, L. Oroszlány, and A. Pályi, *A Short Course on Topological Insulators* (Springer, 2016).